Indoor Localization using Voronoi Tessellation

Mohammad ARIF, Shurjeel WYNE, Syed JUNAID NAWAZ
Department of Electrical Engineering, COMSATS University Islamabad
Islamabad-45550, Pakistan.
shurjeel.wyne@comsats.edu.pk

***Abstract*—Recently the use of received signal strength values from a wireless local area network has received significant research interest for indoor localization. This work investigates a Voronoi-based interpolation method to improve indoor localization performance. The region of interest is spanned by reference measurement locations, termed as *anchors*. The proposed method is shown to outperform well-known localization techniques such as the *k*-Nearest Neighbor (*k*-NN) and the Inverse Distance Weighting (IDW) methods in terms of accuracy and precision. Our results show that for a 20 m × 20 m room the proposed scheme can achieve a location accuracy of 5.7 m with at most 5 anchors, whereas the IDW and *k*-NN techniques attain location accuracies of only 6.1 m and 6.5 m, respectively, under the same conditions. These performance gains are achieved while maintaining the same number of anchors in the system calibration phase for all the considered techniques.**

***Index Terms*—indoor environments, interpolation, radio propagation, simultaneous localization and mapping, wireless LAN.**

I. INTRODUCTION

The advances in computing capabilities of mobile devices have generated significant research interest in indoor localization-based services such as in-building rescue operations, equipment or personnel tracking in hospitals, and guidance for shopping malls and museums [1-3]. The widespread use of wireless local area networks (WLANs) and the minimal requirements for additional localization hardware have made WLAN-based localization an active research area [4-6].

Localization algorithms can be broadly classified as range-based, proximity-based and fingerprinting-based [2]. In the range-based methods such as Time of Arrival (ToA) [7] or Time Difference of Arrival (TDoA) [8] of the received signals, the separation distance between the transmitter (TX) and the receiver (RX) is calculated directly [9]. In proximity-based methods typically employed in wireless sensor networks (WSNs), a node location is estimated in relation to its neighboring nodes without explicitly calculating the TX-RX separation distance [2]. In fingerprinting-based methods, the signals transmitted by multiple access points (APs) can be used for localization of the user equipment (UE). A radio map or fingerprint of the target region is constructed from received signal strength (RSS) values measured at known anchor locations in the calibration phase [10]. In the online phase, the UE's unknown location can be estimated by using some distance metric between the RSS values measured online and the RSS values stored in the radio map [11-13]. It is well-known that the wireless channel significantly affects the WSN performance [14]. Investigations of indoor localization based on ToA and TDoA have shown that these techniques perform poorly due to their requirement of a line-of-sight (LoS) connection, which is difficult to guarantee indoors due to fading [3], and a strict TX-RX time-synchronization that requires expensive hardware [2]. This has led to fingerprinting as the preferred method for indoor localization [3], [15].

A common drawback of fingerprinting-based methods is the significant measurement effort required in constructing the radio map. The system's localization error can be reduced either by adding more anchors or by employing more accurate interpolation in the online phase [16]. The drawback of adding more anchors is the extra burden on system resources for recording and storage of the additional fingerprints. Interpolation based on Voronoi diagrams has also been investigated [17-19]. A Voronoi diagram is a set of polygons that tessellate a target region relative to a set of reference locations [20]. For Voronoi-based localization, the set of anchors constitute these reference locations. A k-th order Voronoi diagram (k-OVD) is defined by a set of polygons whose interiors comprise all spatial points that are closest to k reference points among the set of all reference points [19-20]. In the $k = 1$ case, the number of tessellating polygons equals the number of reference points. For $k > 2$, the k-OVD is referred to as a higher-order Voronoi diagram. In [17], the authors proposed a wireless geolocation technique using joint RSS-based Voronoi diagrams and factor graphs. They used simulation analysis to verify that their proposed approach yielded a root-mean-squared localization error on the order of a few meters. In [18], a first-order Voronoi tessellation was used in conjunction with the Lagrange multiplier method to perform localization in a WSN. In [19], the authors proposed to use a higher-order Voronoi tessellation to construct a radio map of the target site. Their approach yielded better estimates of the signal fading parameters within each Voronoi polygon, which led to a more accurate Wi-Fi radio map construction. Their interpolated radio map was then used for localization with the k-nearest-neighbor (k-NN) technique [15] and the Inverse Distance Weighting (IDW) method of [21].

The novelty of the submitted work in relation to [19] is that we apply a higher-order Voronoi tessellation differently from [19] to solve the indoor localization problem. More specifically, a new set of virtual anchor locations is constructed from the physical anchors associated with each Voronoi polygon. Furthermore, the localization performance is quantified not only in terms of localization accuracy as in [19] but additionally the localization error distribution is also evaluated. We compare our proposed method with the k-NN and IDW localization techniques. Our evaluations

Digital Object Identifier 10.4316/AECE.2018.04010

reveal that the proposed method yields a smaller average value and spread of the localization error in relation to the other two techniques.

The remainder of this paper is organized as follows. In Section 2, we provide some details about the investigated techniques. In Section 3 the system model and performance metrics are described. In Section 4, some numerical results are provided. Finally, Section 5 concludes this paper.

II. Fingerprinting-based Localization

Consider an indoor scenario where localization is to be performed in the horizontal plane. In the calibration phase, RSS values from M transmitting APs are measured at N anchor locations. In the online phase, the Euclidean distance in RSS space is calculated between the unknown UE location and j-th anchor as [2]

$$E_j = \sqrt{\sum_{m=1}^{M} \left(\varphi_{mj} - S_m\right)^2}, \quad j = 1,2,\ldots,N, \tag{1}$$

where φ_{mj} is the RSS from m-th AP measured at j-th anchor in calibration phase and S_m is the RSS from the same AP measured at the unknown UE location in the online phase. The UE location can be estimated, according to the nearest-neighbor (NN) method [11], [15], as the coordinates of the j-th anchor provided that $E_j < E_k, \; \underset{k \neq j}{k = 1,2,...,N}$.

A. k-NN Localization

An obvious limitation of the NN technique is that the estimated UE location is restricted to be one of the anchor locations, which can cause significant localization error. For this reason, interpolation methods such as the k-NN technique have been proposed in the literature, [11], [15]. According to the k-NN method the coordinates of the unknown UE location are estimated as [15]

$$\left(\hat{x}, \hat{y}\right) = \frac{1}{k} \sum_{j=1}^{k} \left(x_j, y_j\right), \tag{2}$$

where $\left(\hat{x}, \hat{y}\right)$ is the estimated UE location and (x_j, y_j) are coordinates of the j-th anchor among the k anchors closest to the UE location in RSS space. The variable k is a system parameter. In other words, the unknown UE location is estimated as an average of the k nearest anchor locations. Note that this technique includes the NN method as the special case $k = 1$, which has no interpolation.

B. Inverse distance weighting localization

A more refined interpolation for the UE location can be obtained by a weighted average of the T closest anchor locations. In the T-IDW technique, these weights are assigned as a decreasing function of the UE's distance to the anchors. The unknown UE location is estimated as [21]

$$\left(\hat{x}, \hat{y}\right) = \frac{\sum_{i=1}^{T} \left(x_i, y_i\right) s_i^{-\gamma}}{\sum_{i=1}^{T} s_i^{-\gamma}}, \tag{3}$$

where s_i is the distance in RSS space between the unknown UE location and the i-th anchor. The system parameters γ and T represent the power law distance dependence and the number of anchors, respectively.

C. Proposed Voronoi-based localization

Consider a 2-D region of interest that is spanned by a set $P = \{p_1, p_2, \ldots, p_N\}$ of N anchors. For ease of exposition, consider tessellation of this region by a second order Voronoi diagram (2-OVD) only. The application to higher orders is straightforward but will not be discussed here to simplify notation. Now the Voronoi polygon associated with the l-th pair of anchors $P_l^{(2)} = \{p_{l,1}, p_{l,2}\}$ can be expressed as [20], [22]

$$V\left(P_l^{(2)}\right) = \{a : d(a, p_{l,1}), d(a, p_{l,2}) \le d(a, p_j), \; \forall p_j \in P \setminus P_l^{(2)}\}. \tag{4}$$

Here l=1, 2…, L, where L is the number of distinct anchor pairs that can be chosen from N, i.e., $L = N!/[2!(N\text{-}2)!]$. Furthermore, a is an arbitrary point in the region of interest and $d(a, p_{l,q})$ is the Euclidian distance between a and the q-th, q = 1, 2, member of the l-th anchor pair $P_l^{(2)}$. Finally, $P \setminus P_l^{(2)}$ denotes the set P after exclusion of the two anchors included in $P_l^{(2)}$. It may be noted that any point in the interior of $V\left(P_l^{(2)}\right)$ is closer to the anchors in $P_l^{(2)}$ than to any other anchors in P. According to the proposed interpolation scheme, in the calibration phase two parameters are calculated for each $P_l^{(2)}$ as follows:

(i) An RSS M-tuple whose m-th entry is computed as

$$\varphi_{ml} = \frac{\left(\varphi_{ml_1} + \varphi_{ml_2}\right)}{2}, m = 1,2,...,M. \tag{5}$$

(ii) A pair of virtual coordinates computed as

$$\left(x_{vl}, y_{vl}\right) = \left(\frac{x_{l_1} + x_{l_2}}{2}, \frac{y_{l_1} + y_{l_2}}{2}\right), \tag{6}$$

where $\left(x_{l_1}, y_{l_1}\right)$ and $\left(x_{l_2}, y_{l_2}\right)$ represent the spatial coordinates of the first and second anchor of $P_l^{(2)}$, respectively. The calculations in (5) and (6) are repeated for each $V\left(P_l^{(2)}\right)$ in the 2-OVD of the target region and the results are stored for subsequent use.

In the online phase, the measured RSS M-tuple's distance to each of the L RSS vectors from (5) is computed according to (1). Finally, the $V\left(P_l^{(2)}\right)$ with the smallest distance to the online M-tuple is selected and its virtual coordinates, computed from (6) are returned as the estimated location of the UE. Thus, the only extra computations are the L distance calculations followed by an arithmetic mean of the anchor pair closest to the UE's RSS M-tuple. These calculations are easily manageable with the computational resources available in today's smart devices.

The proposed method constructs $L \ge N$ virtual anchors spanning the same area as the original N physical anchors.

The localization error is reduced with the proposed approach because the inter-anchor distance between the virtual anchors is, on average, significantly smaller than that between the original N anchors. It may be noted that the k-NN and T-IDW techniques use the original N anchors for localization. Thus, it may be concluded that for the same N the proposed method yields a smaller error than both the k-NN and the T-IDW techniques. This assertion is also validated by the localization performance plots shown later in the numerical results section.

III. System Model

The localization performance is evaluated for two indoor scenarios of practical significance. These scenarios are referred to as setup 1 and 2, respectively, in the remainder of this work. The setup 1 shown in Fig. 1 consists of a 20 m × 20 m room with 4 APs fixed at its corners. The number of anchors can be varied between 5 and 25 but they are assumed to be located on a regular grid [23]. Fig. 2 shows an exemplary tessellation of setup 1 according to the 2-OVD described in Section II, for $N = 5$ anchors. Each polygon shown in Fig. 2 is labelled with an ordered pair that indicates the anchor indices associated with that polygon. For example, the top middle polygon shown in Fig. 2 is labelled with (11, 13). This indicates that all points in the interior of this polygon are closer to anchor number 11 and 13 than to the remaining three anchors. Fig. 3 shows the setup 2, which consists of a 90 m × 90 m area, divided into 9 rooms of identical 30 m × 30 m dimensions. Four APs are fixed at the corners of the 90 m × 90 m area. An identical number of anchors are considered in each room and the total number of anchors can be varied between 9 and 81 while placing them on a regular grid [7].

A. Path loss Model for RSS

The received radio signal experiences fading due to the presence of blocking objects such as furniture and appliances in an indoor environment. In the literature the well-known log-distance path loss model with shadow fading has been used to model the received signal in indoors environments [3], [12], [15]. Furthermore, the extra attenuation due to signal absorption and reflection by room partition walls is often considered by including an additional wall attenuation factor in the received signal model. The received power can then be written as [24],

$$P(d) = P(d_o) - 10n\log\left(\frac{d}{d_o}\right) + X_\sigma - \omega * PAF, \qquad (7)$$

where $P(d)$ is the RSS at TX-RX separation distance d, $P(d_o)$ is the RSS measured at reference distance d_o, taken to be 1 m, and n is the path loss exponent. Furthermore, X_σ is a zero mean Gaussian random variable with standard deviation σ that models fading and PAF is the partition attenuation factor due to a single wall. Finally, ω is the number of intervening walls between TX and RX. Note that in setup 1, $\omega = 0$ due to the absence of walls.

TABLE I. Simulation Parameters used for RSS Model [7]

Parameter	n	$P(d_o)$	σ	PAF
Value	2	-40dBm	3	5

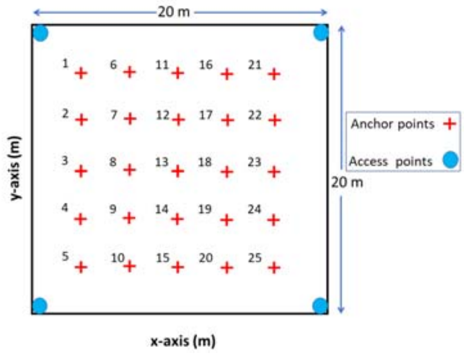

Figure 1. Setup 1 showing anchor points numbered sequentially.

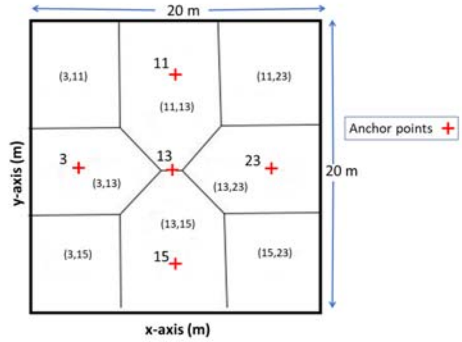

Figure 2. Setup 1 tessellated by a 2-OVD with only 5 anchor locations.

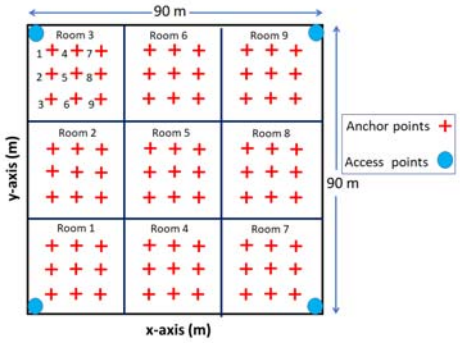

Figure 3. Setup 2. Anchor points are identically numbered in each room.

B. Simulation Methodology

The localization performance was evaluated by the Monte Carlo method and using the Matlab© platform.

For a given placement of anchors and APs, the calibration phase RSS values at each anchor were calculated according to (7). For the online phase, independent Monte Carlo trials were performed such that for each trial the UE was placed randomly according to a uniform distribution. The UE location was then estimated by each of the considered techniques and the respective estimation errors for each trial were recorded. This statistical ensemble was used for analyzing the localization error.

C. Performance Metrics

The performance metrics used for evaluating localization performance of the algorithms are described next.

1) Accuracy

The accuracy of a localization technique is given by the average error between the estimated and the true UE coordinates and expressed as [2],

$$\text{Accuracy} = E\left[\sqrt{(\hat{x} - x_o)^2 + (\hat{y} - y_o)^2}\right], \qquad (8)$$

where $E[.]$ denotes statistical expectation, (x_o, y_o) are the

UE's true location coordinates in online phase and $(\hat{x}, \hat{y})$ are its estimated coordinates.

2) Precision

While accuracy quantifies the average error of a localization technique, precision refers to the distribution of the localization error. A localization technique that exhibits an error distribution concentrated on small error values is preferable because it indicates that this technique is likely to estimate the location with a small distance error. In this work, the empirical cumulative distribution function (CDF) of the localization error is used to evaluate the distribution of the localization error.

IV. NUMERICAL RESULTS

For a fair comparison of localization performance an identical number of anchor locations are used for the considered techniques. For the k-NN algorithm, k values between 2 and 4 have been reported to provide accurate localization [12]. If larger k values are used, then the localization accuracy degrades as more geographically distant anchor locations are introduced into the averaging given in (2). In case of the proposed k-OVD technique, choosing $k >> 2$ for implementing on a mobile device may significantly burden computational resources of the device. In view of these considerations for illustrative purposes we set $k = T = 2$ in our evaluations, i.e., the numerical results compare the performance of the proposed 2-OVD-based localization with the 2-IDW and 2-NN techniques.

In Fig. 4 the average location error and the error spread are plotted as a function of the number of anchor locations, with number of APs fixed at 4. Fig. 4 (a) shows the results for simulation setup 1 whereas Fig. 4 (b) shows the results for simulation setup 2. It can be observed from Fig. 4 that as the number of anchors are increased, the average error for the 2-NN, 2-IDW and 2-OVD techniques reduces but the 2-OVD technique consistently gives smaller average error than the 2-NN and 2-IDW method, e.g., from Fig. 4 (a), it can be seen that for 15 anchor points, the average error with the 2-NN and the 2-IDW techniques is 5.6 m and 4.8 m, respectively. However, with the 2-OVD method the average error is only 4.5 m. From the confidence intervals for the localization error, which are plotted as vertical bars in Fig. 4 (a) and (b), one can observe that the error spread about its average value also decreases with an increasing number of anchors. However, the error spread for the 2-OVD technique is consistently less than that observed for the 2-NN and the 2-IDW techniques.

We have also investigated the effect of increasing the number of APs on the localization error, with number of anchor locations kept constant. The relevant scenario and results are shown in Fig. 5. In Fig. 5 (a) the modified simulation setup 1 is shown. In this case, there are 5 anchor locations and the number of APs is increased from 5 to 8. In Fig. 5 (b) the average error and error spread are plotted. From these plots, it can be observed that by increasing the number of APs the average error and error spread decrease for all three techniques. However, the error values yielded by the 2-OVD technique are consistently less than those obtained by the 2-IDW and 2-NN methods.

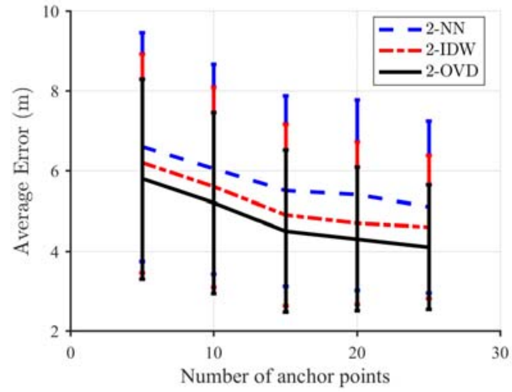

(a)

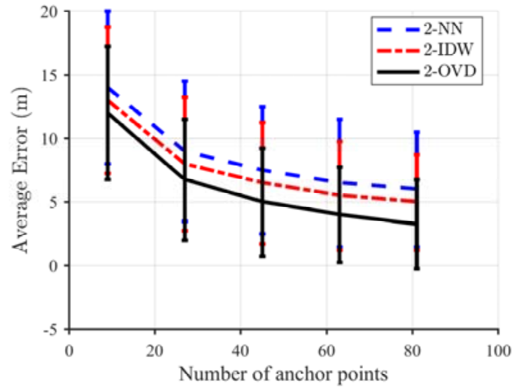

(b)

Figure 4. Average error and error spread as a function of number of anchor points. Number of AP nodes = 4. (a) 20 X 20 m setup (b) 90 X 90 m setup.

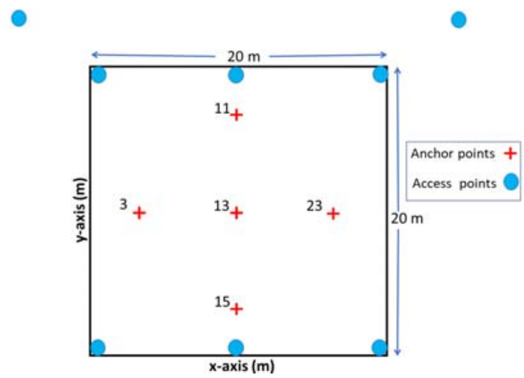

(a)

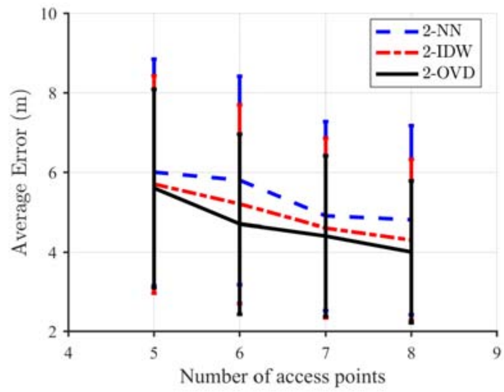

(b)

Figure 5. Modified setup 1 and its error plots. (a) Modified setup 1 (b) Average error and error spread as a function of number of APs. Number of anchor points = 5.

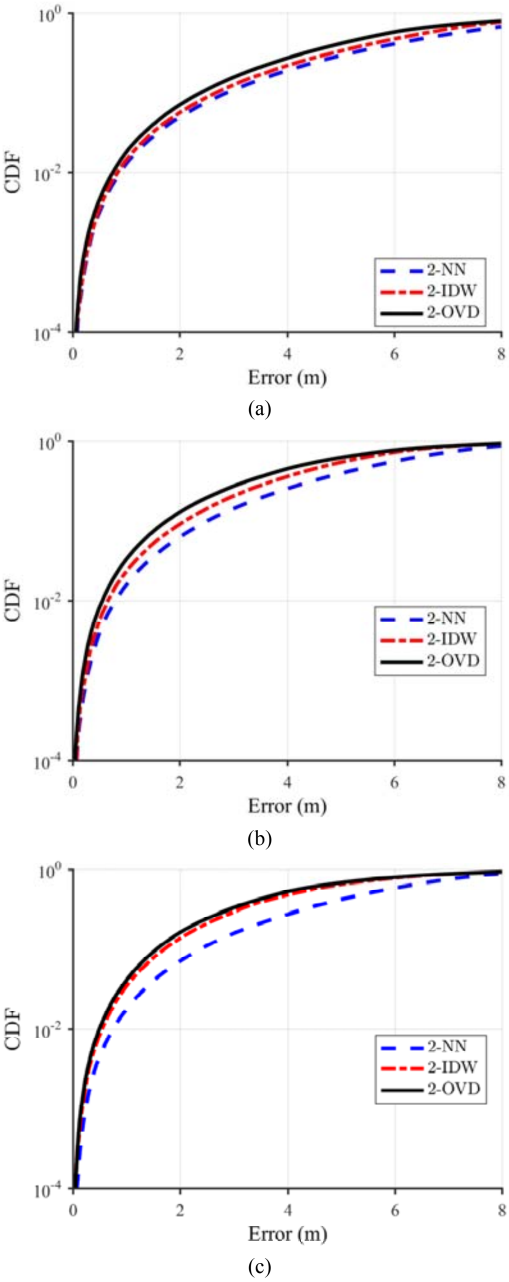

Figure 6. CDF of estimation error for 20 X 20 m setup. Number of AP nodes = 4. (a) 5 Anchor points (b) 15 anchor points (c) 25 anchor points.

The localization precision for 2-OVD, 2-IDW and 2-NN techniques is described by the error CDFs that are plotted in Fig. 6 for simulation setup 1 and in Fig. 7 for simulation setup 2. For both figures, the number of APs is fixed at 4 and the number of anchor locations is varied between each of the Fig. subplots. Considering the results in Fig. 6, the CDFs in Fig. 6 (a) are plotted by considering only 5 anchor locations: no. 3, 11, 13, 15, and 23 as shown in Fig. 2; the CDFs in Fig. 6 (b) are plotted for 15 anchor locations: no. 1, 3, 5, 7-9, 11-15, 17-19 and 21 as shown in Fig. 2; Finally, in Fig. 6 (c) the CDFs are plotted by considering all 25 anchor locations. For better readability, the x-axis in the sub-figures is limited to showing error values up to 8 m.

From Fig. 6 (a), the localization error in 20% of the cases is below 4 m and 3.75 m for the 2-NN and the 2-IDW techniques, respectively. In comparison, the error at the 20th percentile is below 3.4 m for the 2-OVD technique. Note that the CDF of 2-OVD in Fig. 6 (a) is obtained by following the method of Section II with 5 anchors only. From Fig. 6 (b) that considers 15 anchors only, the 2-NN and 2-IDW techniques are observed to have a localization error less than 3.5 m and 3 m, respectively, in 20% of the trials. In contrast, the 2-OVD technique gives an error of 2.5 m or less in 20% of the trials. In Fig. 6 (c), the 2-NN and the 2-IDW techniques show 20th percentile errors of 3.4 m and 2.4 m, respectively. In contrast, the 2-OVD technique shows an error of 2.3 m or less in 20% of the cases. These results indicate that the precision advantage of the 2-OVD technique over the 2-NN and the 2-IDW techniques increases with increasing number of anchors. Furthermore, the error CDF curve for the 2-OVD technique lies above the error CDF for the 2-NN and the 2-IDW technique in all subplots; this indicates that under identical operating conditions the 2-OVD method is more likely to produce small error values than the 2-NN and the 2-IDW techniques.

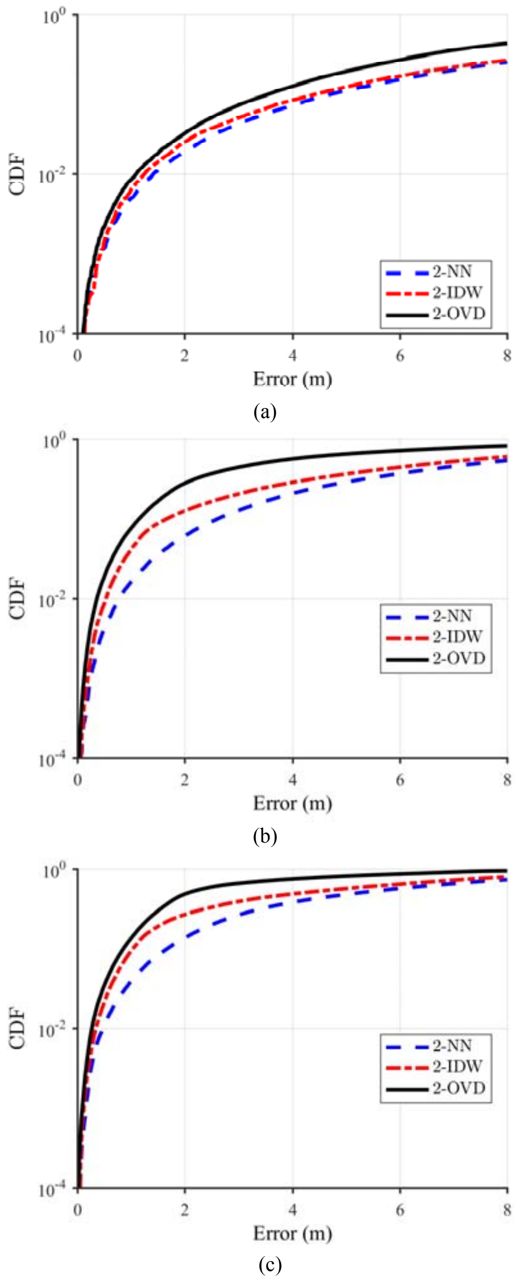

Figure 7. CDF of estimation error for 90 X 90 m setup. Number of AP nodes = 4. (a) 9 anchor points (b) 45 anchor points (c) 81 anchor points.

Now considering the error CDFs in Fig. 7 for simulation setup 2, the CDFs in Fig. 7 (a) are plotted by considering only 9 anchor locations, i.e., using only anchor location no. 5 in each room as shown in Fig. 3; the CDFs in Fig. 7 (b) are plotted by considering only 45 anchor locations, i.e., anchor locations numbers 1, 4-6, and 9 in each of the 9 rooms as shown in Fig. 3. Finally, the CDFs in Fig. 7 (c) are plotted by considering all 81-anchor locations across 9 rooms as shown in Fig. 3. For better readability of plots, the x-axis in all sub-figures is limited to error values of 8 m. In Fig. 7 (a), the 2-NN and the 2-IDW technique are seen to have a localization error at 20-th percentile of 7 m and 6.5 m, respectively. For the 2-OVD technique the localization error is only 5 m at the 20-th percentile. Fig. 7 (b) shows that the localization error in 20% of the trials for 2-NN and 2-IDW techniques is 4 m and 3 m, respectively. In comparison the 2-OVD technique yields localization error of only 1.75 m under the same operating conditions. In Fig. 7 (c), the 2-NN and the 2-IDW techniques give localization errors in 20% of the trials of 3.25 m and 1.5 m, respectively. On the other hand, the 2-OVD technique gives a localization error of only 1.25 m. The general trend indicated by Fig. 6 and 7 is that the proposed 2-OVD technique can provide location estimates within a room resolution, with much higher reliability than the 2-NN and 2-IDW.

V. Conclusion

We have compared localization performance of the proposed Voronoi-based interpolation technique with the *k*-NN and *T*-IDW methods using RSS values in two indoor scenarios. The mean localization error and the error spread are reduced by increasing the number of anchor locations for 2-NN, 2-IDW and 2-OVD techniques but the error values for the 2-OVD technique were shown to be consistently less than those for the 2-NN and the 2-IDW methods. It was also demonstrated that for a fixed number of anchor locations, the mean error and the error spread both decrease by increasing the number of APs, but again the 2-OVD technique consistently gives lesser error values than the 2-NN and 2-IDW techniques. The distribution of localization error was also investigated for 2-NN, 2-IDW and 2-OVD techniques; it was shown that under identical operating conditions, the proposed 2-OVD method is more likely to give smaller distance errors than the 2-NN and the 2-IDW methods. Our results show that the proposed *k*-OVD technique can provide location estimates within a room resolution, with much higher reliability than the *k*-NN and the *T*-IDW techniques under identical operating conditions.

References

[1] D. Li, Y. Yan, B. Zhang, C. Li and P. Xu, "Measurement-based AP deployment mechanism for fingerprint-based indoor location systems," KSII Transactions on Internet and Information Systems, vol. 10, no. 4, pp. 1611-1629, 2016. doi: 10.3837/tiis.2016.04.008

[2] R. Zekavat and R. M. Buehrer, "Handbook of position Location: Theory, Practice and Advances", IEEE Series on Digital and Mobile Communication, Wiley-IEEE Press, 2011.

[3] A. Yassin, Y. Nasser, M. Awad, A. Al-Dubai, R. Liu, C. Yuen, R. Raulefs and E. Aboutanios, "Recent advances in indoor localization: A survey on theoretical approaches and applications," IEEE Communications Surveys & Tutorials. Vol. 19, no. 2, pp. 1327-1346, 2016. doi: 10.1109/COMST.2016.2632427

[4] W. Zhao, S. Han, W. Meng, and D. Zou, "A testbed of performance evaluation for fingerprint based WLAN positioning system," KSII transaction on internet and information systems, vol. 10, no. 6, pp. 2583-2605, 2016. doi: 10.3837/tiis.2016.06.008

[5] D. Han, S. Jung, M. Lee, and G. Yoon, "Building a practical Wi-Fi-based indoor navigation system," IEEE Pervasive Computing, vol. 13, no. 2, pp. 72-79, 2014. doi: 10.1109/MPRV. 2014.24

[6] Y. Mo, Z. Zhang, Y. Lu, and G. Agha, "A novel technique for human traffic based radio map updating in Wi-Fi indoor positioning systems," KSII Transactions on Internet and Information Systems, vol. 9, no. 5, pp. 1881-1903, 2015. doi: 10.3837/tiis.2015.05.019

[7] J. Yang and Y. chen, "Indoor localization using improved RSS-based Lateration methods," in Proc. 28th IEEE conference on Global telecommunications, 2009. doi: 10.1109/GLOCOM.2009.5425237

[8] C. R. Comsa, J. Luo, A. Haimovich, and S. Schwartz, "Wireless localization using time difference of arrival in narrow-band multipath systems," in Proc. International symposium on signals circuits and systems, Romania, 2007. pp. 1-4. doi: 10.1109/ISSCS.2007. 4292764

[9] C. D. Flora and M. Hermersdorf, "A practical implementation of indoor location-based services using simple Wi-Fi positioning," Journal of location based services, vol. 2, no. 2, pp. 87-111, 2008. doi: 10.1080/ 17489720802415205

[10] P. A. Zandbergen. "Comparison of WiFi positioning on two mobile devices," Journal of Location Based Services, vol. 6, no. 1, pp. 35-50, 2011. doi: 10.1080/17489725.2011.630038

[11] P. Bahl and V. N. Padmanabhan, "RADAR: an in-building RF-based user location and tracking system," in Proc. 9th Annual Joint Conference of the IEEE Computer and Communications Societies, 2000, pp. 775-784. doi: 10.1109/INFCOM.2000.832252

[12] P. Mirowski, P. Whiting, H. Steck, R. Palaniappan; et al., "Probability kernel regression for Wi-Fi localization," Journal of Location based Services, vol. 6, no. 2, pp. 81-100, 2012. doi: 10.1080/17489725.2012.694723

[13] B. Kobben, "Wireless Campus LBS, A Test Bed for Wi-Fi positioning and location based services," Cartography and Geographic Information Science, vol. 34, no. 4, pp. 285-292, 2007. doi: 10.1559/ 152304007782382936

[14] V. C. Gungor and M. K. Korkmaz, "Wireless link-quality estimation in smart grid environments," International Journal of Distributed Sensor Networks, vol. 8, no. 2, 2012. doi:10.1155/2012/214068

[15] D. Wu, Y. Xu, and L. Ma, "Research on RSS based Indoor Location Method," in Proc. IEEE Pacific-Asia Conf. on Knowledge Engineering and Software Engineering, Jan. 2010, pp. 205-208. doi: 10.1109/KESE.2009.67

[16] N. Hernández, A. Hussein, D. Cruzado, I. Parra, and J. M. Armingol. "Applying low cost WiFi-based localization to in-campus autonomous vehicles," in Proc. 20th IEEE International Conference on Intelligent Transportation Systems (ITSC), 2017, pp. 1-6. doi: 10.1109/ITSC.2017.8317780

[17] M. R. K. Aziz, L. Yuto and T. Matsumoto, "A New RSS-based Wireless Geolocation Technique Utilizing Joint Voronoi and Factor Graph," International Journal of Simulation: Systems, Science and Technology, 2016. doi: 10.5013/IJSSST.a.17.32.09

[18] F. Shang, Y. Jiang, A. Xiong, W. Su and L. He. "A Node Localization Algorithm Based on Multi-Granularity Regional Division and the Lagrange Multiplier Method in Wireless Sensor Networks," Sensors, vol. 16, no. 11, 2016. doi: 10.3390/s16111934

[19] M. Lee and D. Han, "Voronoi Tessellation based interpolation method for Wi-Fi radio map," IEEE Communications Letters, vol. 16, no. 3, pp. 404-407, 2012. doi: 10.1109/LCOMM.2012. 020212.111992

[20] F. Aurenhammer, "Voronoi diagrams a survey of a fundamental geometric data structure," ACM Computing Surveys, vol. 23, no. 3, pp. 345–450, 1991. doi: 10.1145/116873.116880

[21] S. P. Kuo and Y. C. Tseng, "Discriminant minimization search for large scale RF based localization systems," IEEE Transaction on Mobile Computing, vol. 10, no. 2, pp. 291-304, 2011. doi: 10.1109/ TMC.2010.67

[22] A. Okabe, B. Boots, K. Sugihara, and S. N. Chiu, "Spatial Tessellations: concepts and applications of Voronoi diagram," 2nd. West Sussex: John Wiley & Sons, 2000.

[23] Z. Xiong, F. Sottile, M. A. Spirito and R. Garello, "Hybrid Indoor Positioning Approaches Based on WSN and RFID," in Proc. 4th IFIP International Conference on New Technologies, Mobility and Security, 2011, pp. 1-5. doi: 10.1109/NTMS.2011.5721059

[24] Y. Seidel and T. S. Rappaport, "914 MHz path loss prediction model for indoor wireless communication in multi-floored buildings," IEEE Transactions on Antennas and Propagation, vol. 40, no. 2, pp. 201-217, 1992. doi: 10.1109/8.127405